Supporting Information

Deciphering the Electrocatalytic Activity of Nitrogen-Doped Carbon Embedded with Cobalt Nanoparticles and the Reaction Mechanism of Triiodide Reduction in Dye-Sensitized Solar Cells

Sung Hee Ahn,[†,#] Chi Ho Lee,[†,#] Min Soo Kim,[†] Seul Ah Kim,[†] Byungwuk Kang,[†] Hee-eun Kim,[†] Sang Uck Lee,[†,‡,] and Jin Ho Bang[†,‡,*]*

Department of Bionano Technology and Department of Chemical and Molecular Engineering, Hanyang University, 55 Hanyangdaehak-ro, Sangnok-gu, Ansan, Gyeonggi-do 15588, Republic of Korea

AUTHOR INFORMATION

Corresponding Authors: Jin Ho Bang, Sang Uck Lee

*Email: jbang@hanyang.ac.kr (J.H.B), sulee@hanyang.ac.kr (S.U.L.)

[†] Department of Bionano Technology, Hanyang University

[‡] Department of Chemical and Molecular Engineering, Hanyang University

[#] These authors contributed equally to this work.

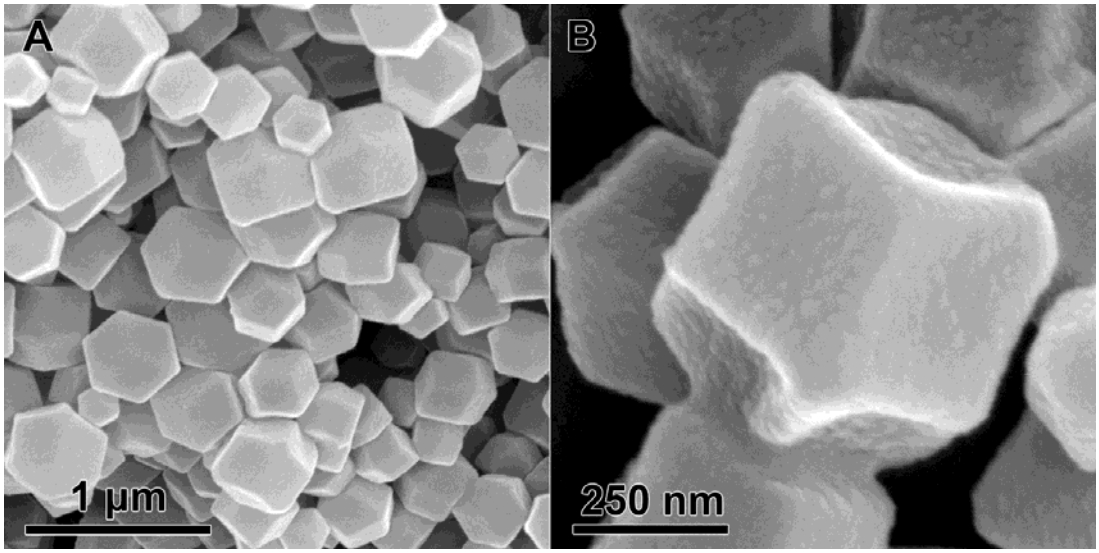

Figure S1. SEM images of ZIF-67 at (A) low magnification and (B) high magnification.

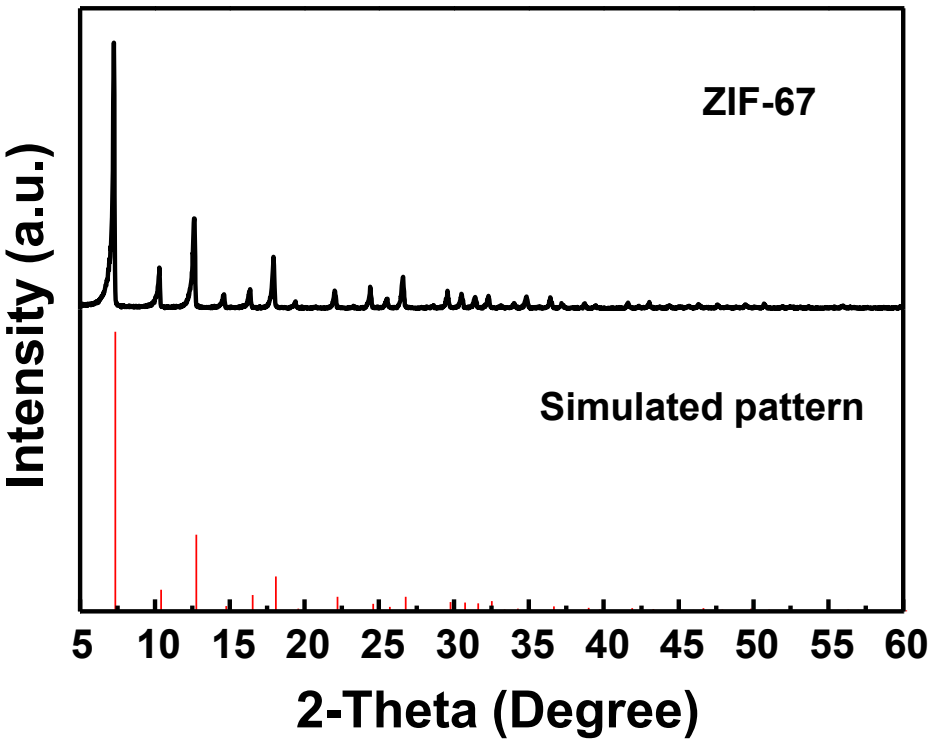

Figure S2. XRD patterns (top: measured, bottom: simulated) of ZIF-67.

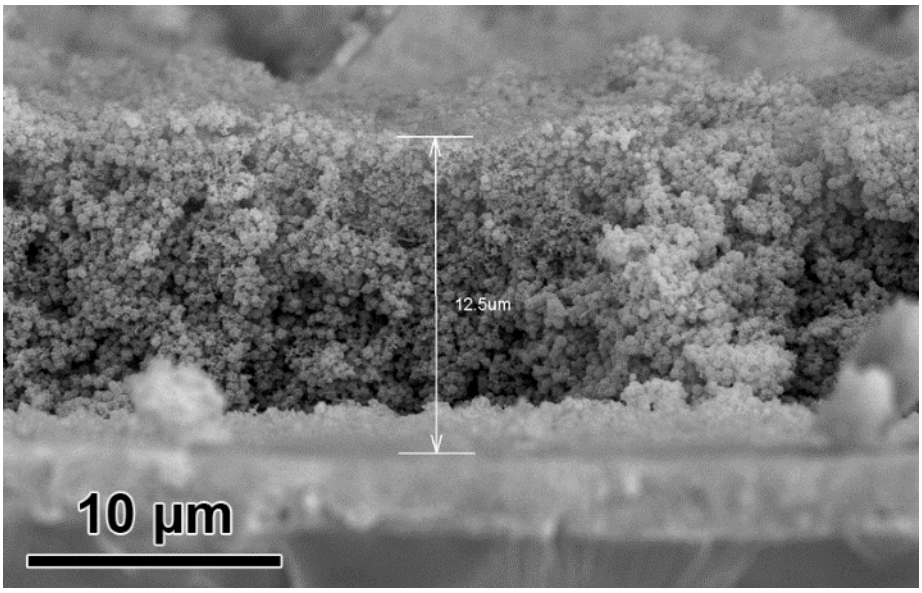

Figure S3. Cross-sectional SEM image of Co/N-C counter electrode.

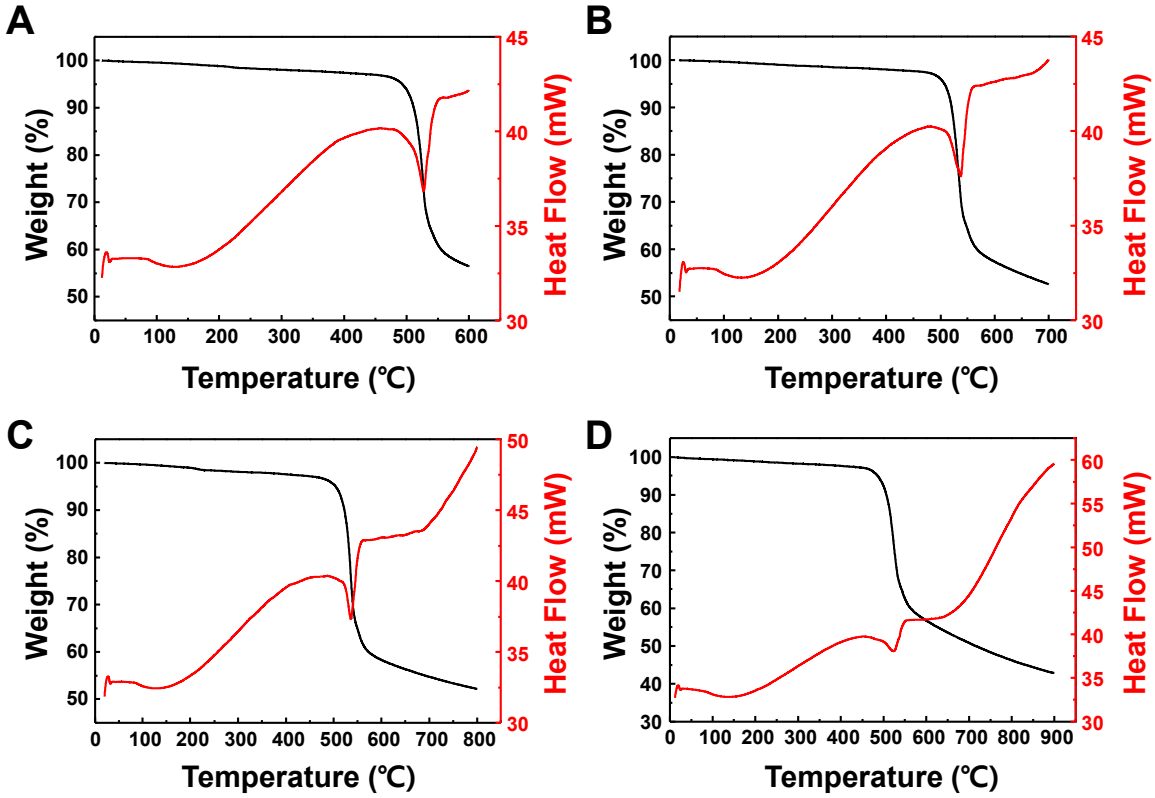

Figure S4. TGA (black lines) and DSC (red lines) analyses of ZIF-67 at different carbonization temperatures.

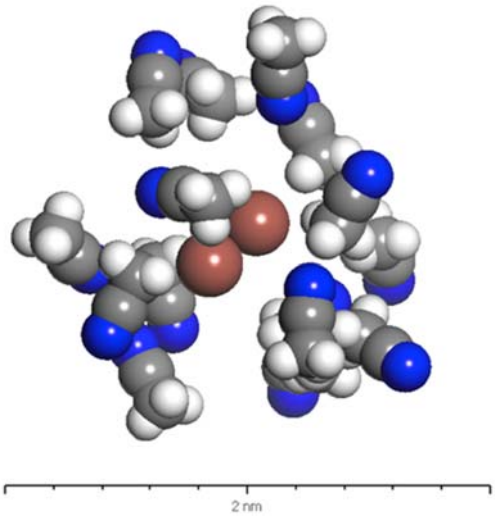

Figure S5. A model of solvated I_2 in CH_3CN. Note that $I_3^- \leftrightarrow I_2 + I^-$ reaction is so fast that all the species are considered to be in equilibrium.

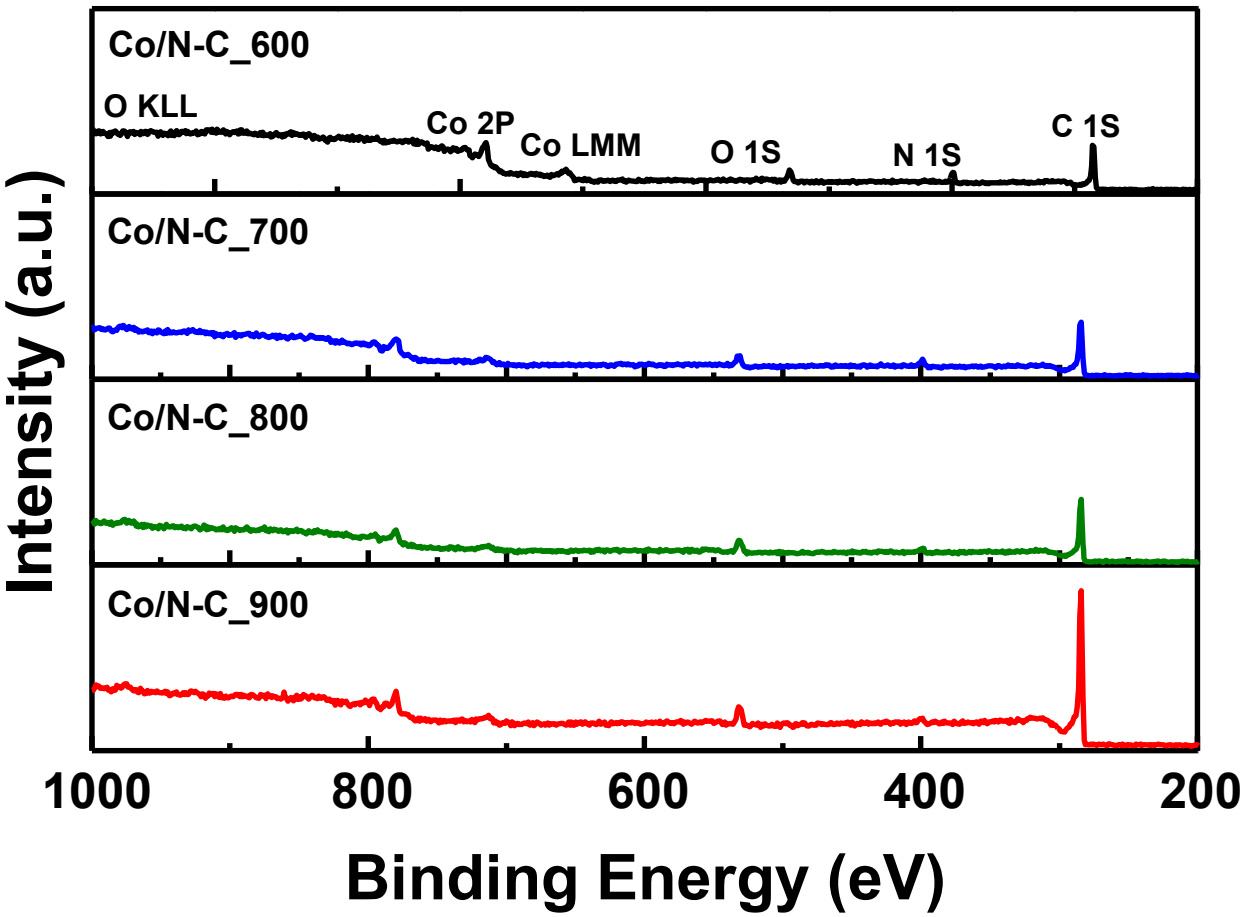

Figure S6. XPS survey spectra of Co/N-Cs obtained at different carbonization temperatures.

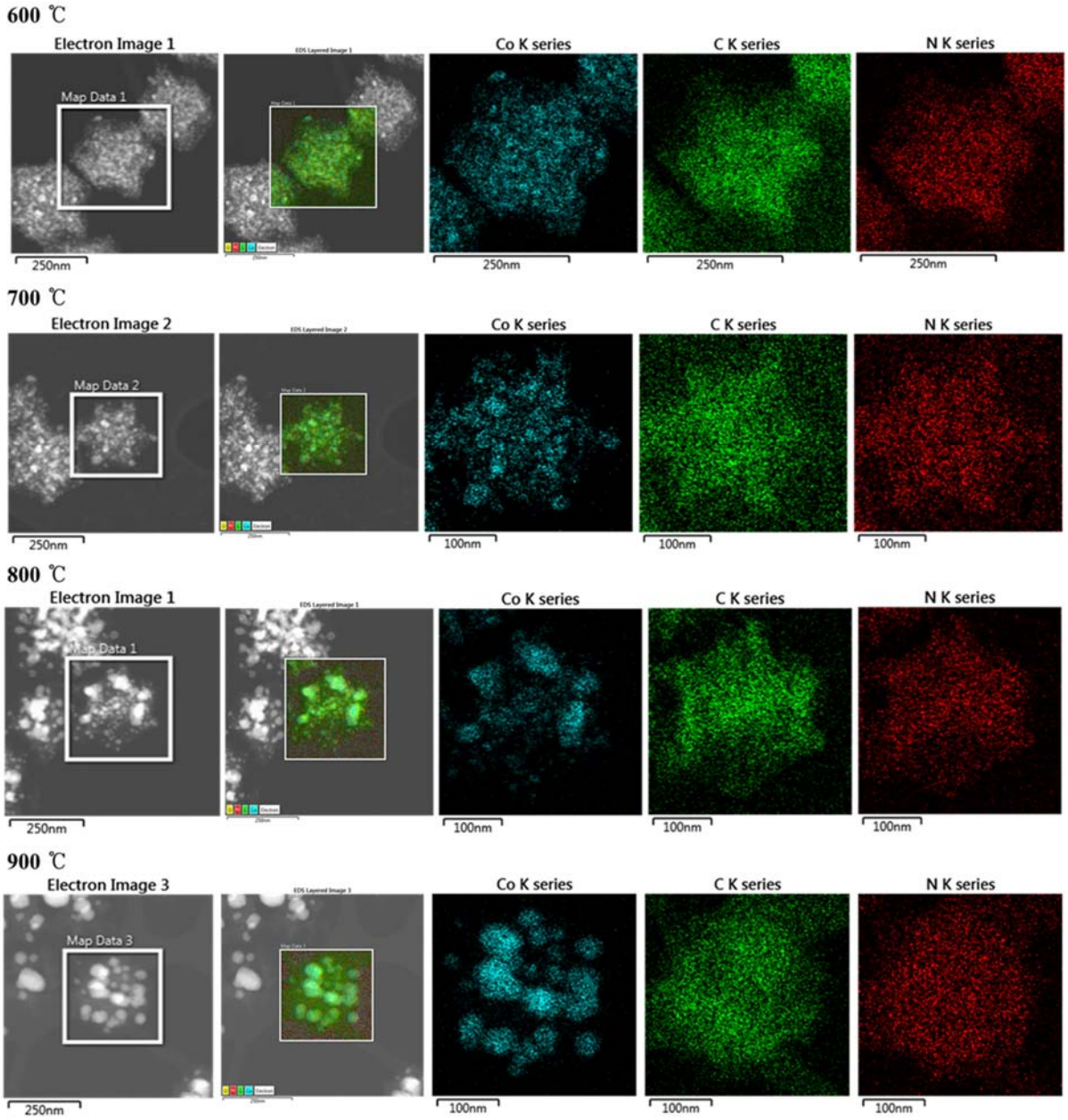

Figure S7. TEM-EDS mapping analysis of Co/N-Cs obtained at different carbonization temperatures.

Table S1. Solar Cell Parameters of DSSCs (multiple cells) with CEs made of Co/N-C obtained at different carbonization temperatures.

Counter electrode	J_{sc} (mA/cm^2)	V_{oc} (V)	FF	η (%)
Co/N-C_600 (Cell 1)	15.59	0.75	0.63	7.39
Co/N-C_600 (Cell 2)	15.50	0.75	0.64	7.42
Co/N-C_600 (Cell 3)	15.55	0.75	0.64	7.41
Co/N-C_700 (Cell 1)	16.75	0.75	0.62	7.78
Co/N-C_700 (Cell 2)	16.84	0.75	0.62	7.81
Co/N-C_700 (Cell 3)	16.81	0.75	0.62	7.79
Co/N-C_800 (Cell 1)	15.55	0.74	0.66	7.59
Co/N-C_800 (Cell 2)	15.46	0.74	0.66	7.55
Co/N-C_800 (Cell 3)	15.93	0.74	0.65	7.66
Co/N-C_900 (Cell 1)	15.30	0.76	0.64	7.40
Co/N-C_900 (Cell 2)	15.39	0.76	0.63	7.41
Co/N-C_900 (Cell 3)	15.37	0.76	0.63	7.39

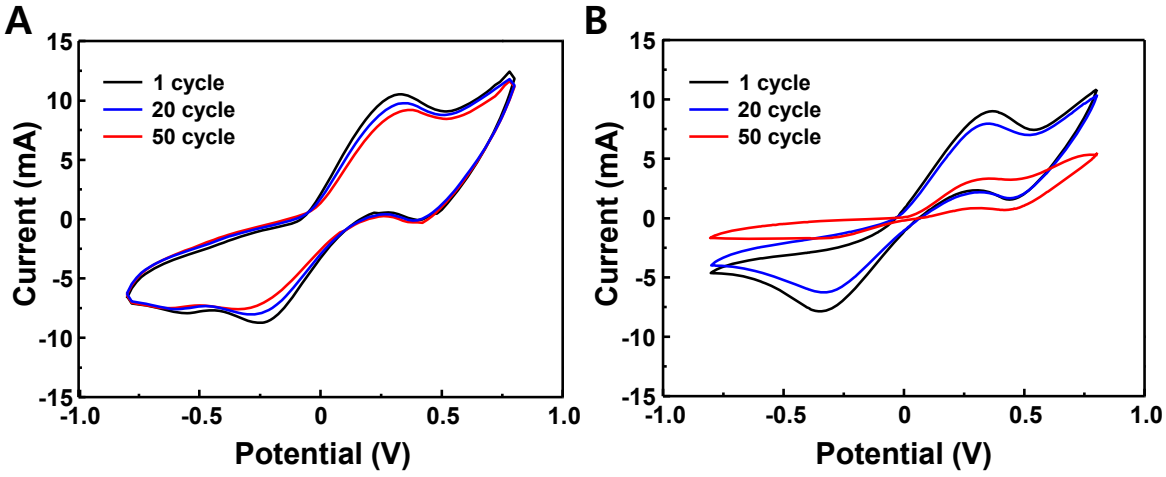

Figure S8. Cyclic voltammograms of (A) Co/N-C_700 and (B) Pt recorded at 100 mV/s in an electrolyte containing 50 mM LiI, 10 mM I_2, and 500 mM $LiClO_4$ in acetonitrile.

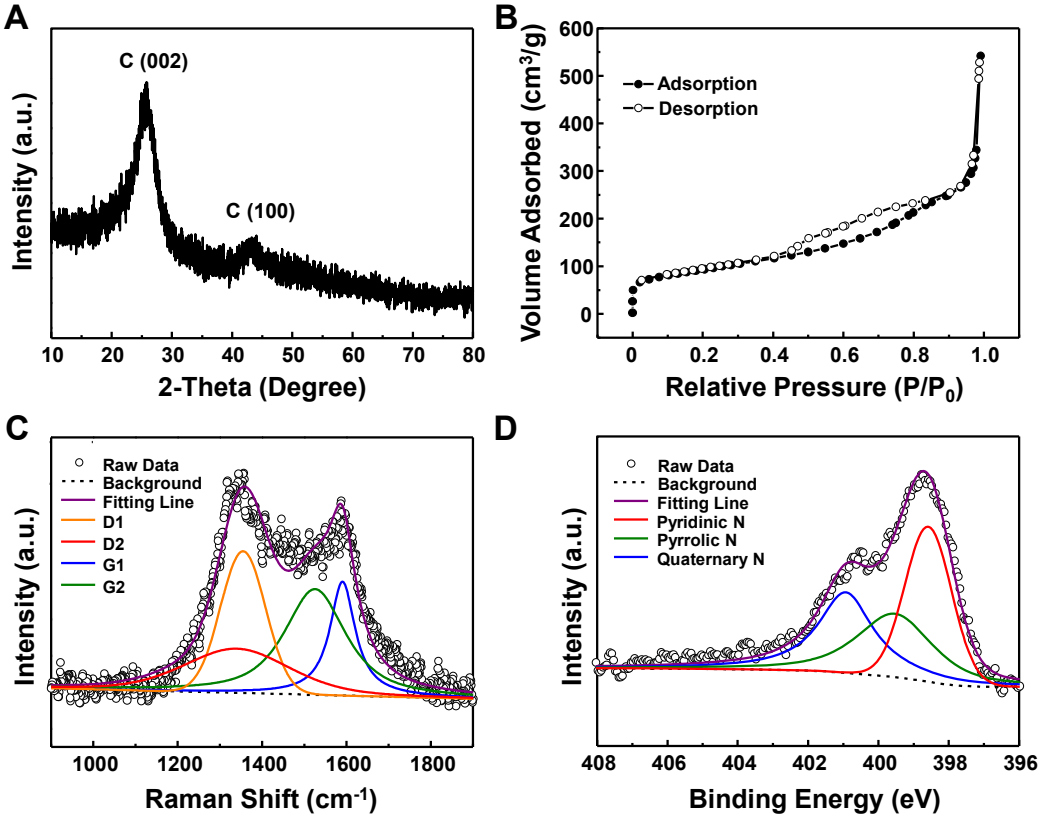

Figure S9. (A) XRD pattern, (B) N_2 physisorption isotherm, (C) Raman spectrum, and (D) XPS N 1s spectrum of N-C_600-700.

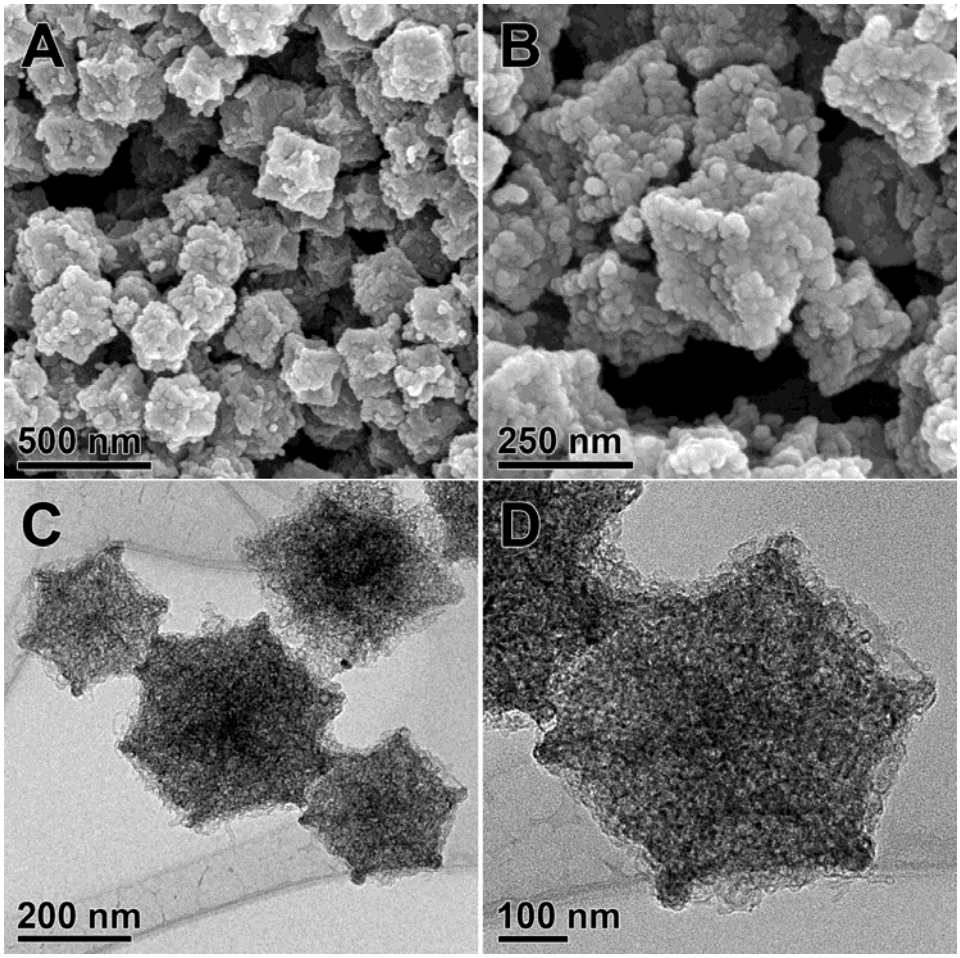

Figure S10. (A, B) SEM images, (C, D) TEM images of N-C_600-700.

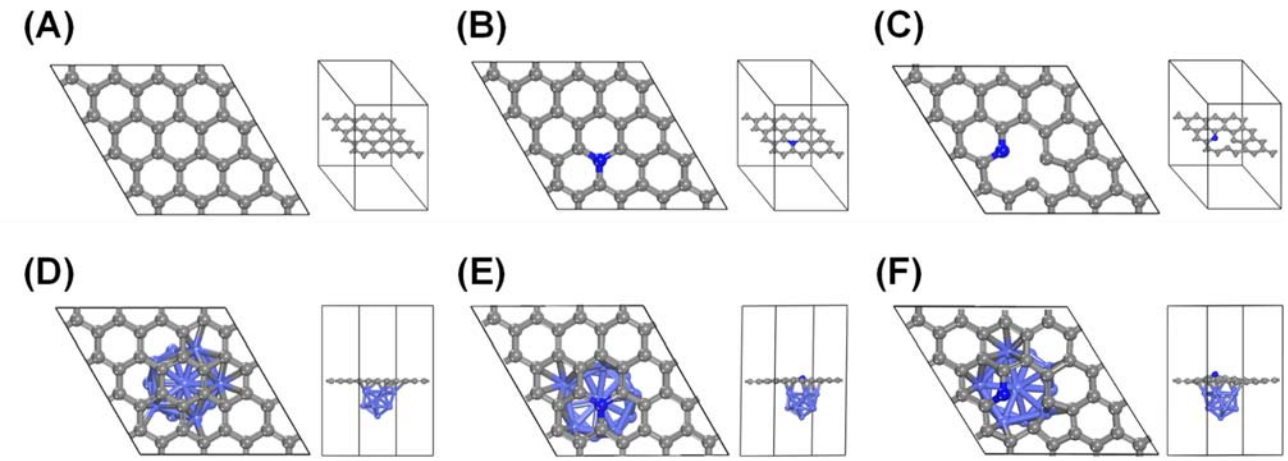

Figure S11. Optimized structures of (A) graphene (G), (B) graphitic nitrogen-doped graphene (gN-G), (C) pyridinic nitrogen-doped graphene (pN-G), (D) graphene incorporating cobalt nanoparticle (G_Co_{12}), (E) graphitic nitrogen-doped graphene incorporating cobalt nanoparticle (gN-G_Co_{12}), and (F) pyridinic nitrogen-doped graphene incorporating cobalt nanoparticle (pN-G_Co_{12}). Note that we considered only basal nitrogen species to elucidate the effect of different types of nitrogen in this work. To consider edge nitrogens, one should use a graphene ribbon model having complex edge structures (e.g., armchair, zigzag, and various types of possible edge termination) that can affect the IRR activity. While the edge nitrogens are also the active site, theoretical calculations based on the complex graphene ribbon model require unimaginably tremendous computation efforts and even makes it difficult to reach a concise, intuitive conclusion. Because of the demand of vast calculations, we computed the dependency of IRR activity on the nitrogen using the consistent periodic model structures. Despite the use of this simplied model, our theoretical results are in good agreement with the previous reports explaining the nitrogen effect, which validates our theoretical approach.

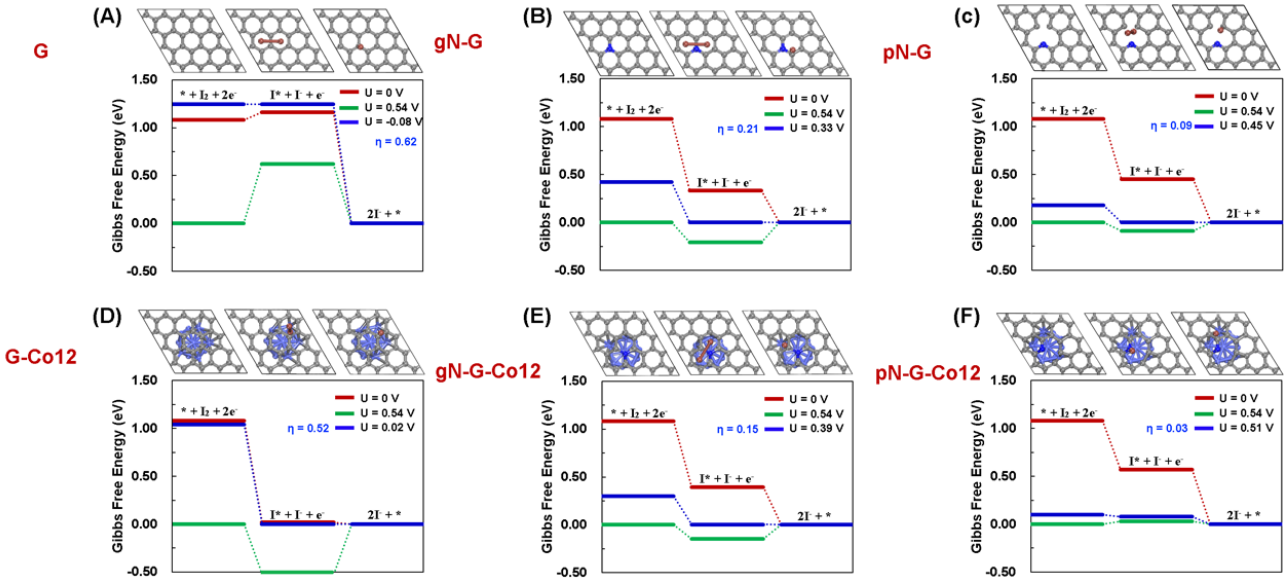

Figure S12. Free energy diagrams and intermediate structures (*I**) of (A) G, (B) gN-G (C) pN-G, (D) G_Co12, (E) gN-G_Co12, and (F) pN-G_Co12 during the IRR pathway. η is the overpotential for overall downhill reaction with respect to the equilibrium reduction potential of I_2 (U=0.54 V).

Table S1. Overpotentials on Graphene-Based Catalysts in the Consecutive IRR Mechanism and the Adsorption Energies of I^- on Graphene-Based Catalysts in the Concerted IRR Mechanism.

Catalysts	Consecutive IRR (Overpotential (η))	Concerted IRR (Iodine adsorption energy (ΔG_{ads}))
G	0.62 eV	1.27 eV
gN-G	0.21 eV	0.37 eV
pN-G	0.09 eV	0.55 eV
G_Co_{12}	0.52 eV	0.36 eV
gN-G_Co_{12}	0.15 eV	0.10 eV
pN-G_Co_{12}	0.03 eV	0.43 eV

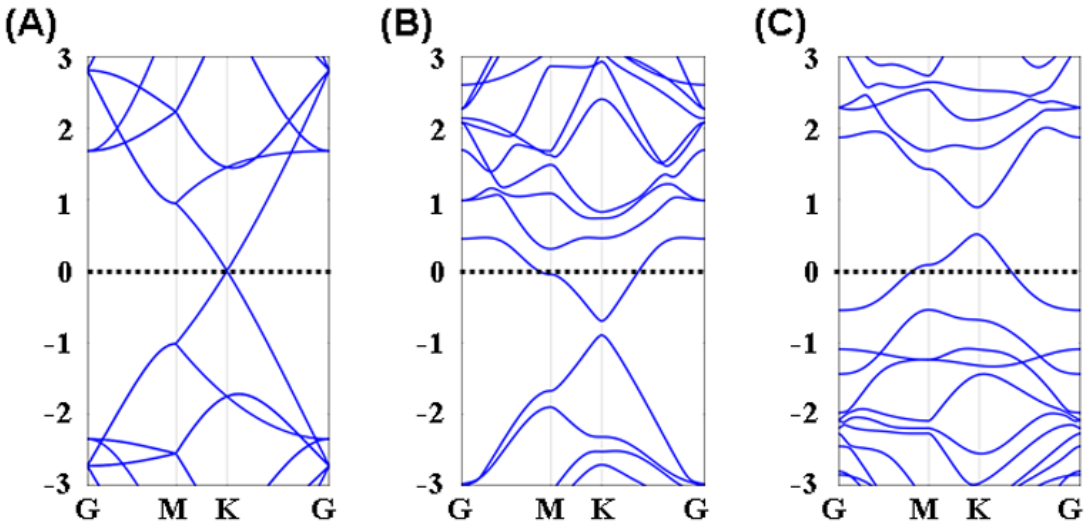

Figure S13. Band structures of (A) graphene (G), (B) graphitic nitrogen-doped graphene (gN-G), and (C) pyridinic nitrogen-doped graphene (pN-G).

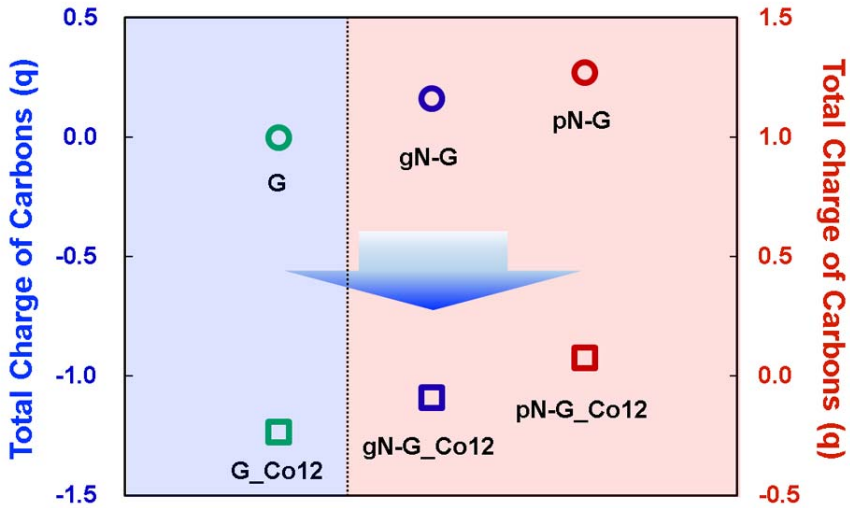

Figure S14. Total charge of C atoms based on the Bader charge analysis for G, gN-G, pN-G, G_Co_{12}, gN-G_Co_{12}, and pN-G_Co_{12}, respectively. The incorporation of Co clusters decreases the carbon charge more negatively. Note that blue region (for G) and red region (for gN-G and pN-G) have different y-axis scales for better visibility.